Applied Surface Science 521 (2020) 146456

Contents lists available at ScienceDirect

Applied Surface Science

journal homepage: www.elsevier.com/locate/apsusc

Design of tetracene-based metallic 2D carbon materials for Na- and K-Ion batteries

Umer Younis[a], Imran Muhammad[a], Yoshiyuki Kawazoe[b,c], Qiang Sun[a,d,*]

[a] Department of Material Science and Engineering, College of Engineering, Peking University, Beijing 10087, China
[b] New Industry Creation Hatchery Center, Tohoku University, Sendai 980-8577, Japan
[c] Suranaree University of Technology, Nakhon Ratchasima, 30000, Thailand
[d] Center for Applied Physics and Technology, Peking University, Beijing 10087, China

ARTICLE INFO

Keywords:
C18
C36H8
Na and K ion batteires

ABSTRACT

Inspired by the tunable electronic properties and high charge carrier mobility of recently synthesized tetracene-based nanoribbons (TNRs) [*Chem. Eur. J.* 2019, 25, 12074], for the first time we design two dimensional (2D) metallic carbon materials by using tetracene (T) as a basic building block. Based on first-principles calculations, we show that the resulting metallic 2D carbon allotropes namely C_{18} and $C_{36}H_8$ are dynamically and thermally stable. Moreover, the porous $C_{18}/C_{36}H_8$ sheets have multiple adsorption sites with strong binding energies for Na/K ions and exhibit a high storage capacity of 991.82/1277.93 mAh/g, low voltage of 0.12/0.46 V and low energy barriers 0.46/0.029 eV respectively. These remarkable findings suggest the applicability of metallic carbon allotropes C_{18} and $C_{36}H_8$ as promising anode materials for Na- and K-ion batteries.

1. Introduction

Two dimensional (2D) porous materials have received remarkable attention because of their outstanding features such as, large surface area, unique optical, electrical, thermal and mechanical properties [1–5], which enable them as a promising candidate for various applications including nanoelectronic devices [6–8], energy storage systems, adsorption [9,10], separation [11,12], and catalysis [13,14]. Among various porous materials, carbon display diverse properties ranging from insulating to semiconducting and to metallic with unprecedented applications [15]. Especially, metallic carbon can exhibit excellent rate performance as anode materials for lithium-ion batteries (LIBs) including Ψ-graphene [16], popgraphene [17], Net-W [18], Net-τ [19], and Hex-C_{18} [20]. Recently, Na and K-ions batteries have received extensive attention, due to the limited Li resources. However, because of the large size of Na and K, the electrode working in Li-ion battery usually doesn't work in Na- and K-ion batteries [21]. Therefore, it is highly desirable to design new metallic carbon materials that can work for Na and K-ions with high performance. As reported earlier, metallic carbon can be designed by using different structural units like T-6 and T14 carbon [15], phagraphene [22], net-W [23], HOP grapheme [24], $H_{5\text{-}6\text{-}7}$ haeckelite [25], C_{65}-sheet [26], OPGZ [27], and T-graphene [28]. Most recently, a new carbon unit (named tetracene) was synthesized through the bottom-up method which shows the ambipolar charge-transport character and indirect band gap [29], it can be used as the unit for one dimensional (1D) [30] and 2D materials [31]. The recent report on the tetracene-based 2D sheet shows the *semiconducting* character [31]. Here, an interesting question arises: Can we design tetracene-based *metallic* 2D sheets? And how good are these tetracene-based metallic 2D sheets for Na and K-ion batteries?

In present work, we design new metallic 2D tetracene-based porous sheets C_{18} and $C_{36}H_8$ with the basic building block of synthesized tetracene (T) [29]. The newly predicted allotropes $C_{18}/C_{36}H_8$ are thermally and dynamically stable and exhibit high storage capacity, faster ions kinetics and low average voltage for Na/K ions. These excellent features together with rich abundance and light mass of carbon proposed the 2D porous C_{18} and $C_{36}H_8$ promising candidate for battery applications.

2. Computational detail

First-principles calculations are performed by using the Vienna *Ab-initio* Simulation Package on the basis of density functional theory [32]. The projector augmented wave (PAW) method is used for electron-ion interaction with a cutoff energy of 600 eV, and Perdew-Burke-Ernzerhof functional (PBE) for electron-electron exchange—correlation [33]. For improving electronic band structure calculations, we also use the hybrid Hyed-Seuseria-Ernzerhof (HSE06) method [34] Monkhorst-Pack

* Corresponding author.
E-mail address: sunqiang@pku.edu.cn (Q. Sun).

https://doi.org/10.1016/j.apsusc.2020.146456
Received 1 February 2020; Received in revised form 13 March 2020; Accepted 4 April 2020
Available online 25 April 2020
0169-4332/

scheme [35] is used with the mesh size of (5 × 12 × 4) and (3 × 8 × 4) for C_{18} and $C_{36}H_8$ structures, respectively. The conjugate gradient method is employed with convergence criteria of 10^{-6} eV, 10^{-3} eV, for energy and force to optimize the geometry. The semi-empirical correction of Gimme PBE-D3 [36] scheme is used for van der Waals (VdW) interactions. Furthermore, the adsorption behavior of metal ions (Na/K) is investigated on C_{18} and $C_{36}H_8$ substrate in the same mesh size. The Bader charge analysis and climbing-image nudged elastic band (CI-NEB) [37,38] techniques are used to study the charge population analysis and diffusion barrier of metal ion on the porous carbonous sheets respectively. In order to confirm the structural and dynamic stability, of porous sheets, the finite displacement method as discussed in phonopy code [39] and *ab initio* molecular dynamics (AIMD) [40] simulation is used in a 3 × 3 × 1 supercell.

3. Results and discussion

3.1. Geometry

The new metallic carbon allotropes C_{18} and $C_{36}H_8$ are constructed by simply repeating the tetracene unit along x and y-direction. "The porous 2D C_{18} contains only carbon atoms and is composed of 4-6-8 carbon rings with Pmmm symmetry (space group D^1_{2h}), while the $C_{36}H_8$ contains 4-6-18 carbon rings with Pmna symmetry (space group D^7_{2h})". The optimized lattice parameters of C_{18} and $C_{36}H_8$ are (a = 11.23 b = 4.33 Å c = 14 Å) and (a = 18.81 b = 6.72 Å c = 14 Å) respectively as shown in Fig. 1(a,b). The distinctive bond lengths between two carbon atoms in cyclobutadiene moieties for C_{18} and $C_{36}H_8$ are 1.40 Å and 1.46 Å while the bond length between carbon and hydrogen atoms in $C_{36}H_8$ sheet is 1.08 Å. As a porous structure, the C_{18} exhibits tetragonal, hexagonal and octagonal rings in its geometry, while $C_{36}H_8$ shows tetragonal, octagonal and a big pore in its structure. In order to analyze the geometry of our porous carbonous allotropes with the previously reported structures, we summarize the results in Table. 1.The planer density for C_{18} and $C_{36}H_8$ sheets are 0.36 atom/Å^2 and 0.34 atom/Å^2 respectively which are slightly less than graphene (0.38 atom/Å^2) and greater than phagraphene (0.29 atom/ Å^2), alpha graphyne (0.187 atom/Å^2) and gamma graphyne 0.288 atom/Å^2) [22].

3.2. Stability

To explore the stabilities of metallic C_{18} and $C_{36}H_8$ sheets, we first calculate the phonon spectrum of both carbonous allotropes by using phonopy code. The phonon spectra displayed in Fig. S1(a, b) of the supplementary information (SI), describes that there is no imaginary part over the whole Brillion zone, which ensures the dynamic stability of C_{18} and $C_{36}H_8$. For thermal stabilities of under discussion porous carbonous sheets, the AIMD simulation is employed for 6 ps with 1 fs time step in 3 × 3 × 1 supercell. The AIMD results displayed in Fig. S1(c, d) illustrates that both allotropes are stable up to 1000 K with a small fluctuation in potential energy. After further analyzing these sheets at higher temperatures the C_{18} found to be more stable which can bear up to 3000 K, results are presented in Fig. S2 of SI. In order to get more inside about the energy stability, we calculate the total energy per atom for both sheets. The total energy of C_{18}-sheet is (−9.046 eV per atom) which is greater than popgraphene (−8.97 eV per atom) [17], penta-graphene (−8.32 eV per atom) [43] and phagraphene (−9.03 eV per atom)[22] while the total energy of $C_{36}H_8$-sheet is (-7.87 eV per atom) which is quite smaller than all these structures.

Table 1
Comparison of tetracene-based metallic 2D carbon with other 2D metallic carbon including types of rings, lattice nature, and electronic band structure.

2D-Carbon structures	Types of rings	Lattice	Band structure
C_{18}-sheet	4 + 6 + 8	orthorhombic	Metallic
$C_{36}H_8$-sheet	4 + 6 + 18	orthorhombic	Metallic
Net-τ[19]	4 + 5 + 6 + 8 + 10	orthogonal	Metallic
biphenylene[23]	4 + 6 + 8	orthogonal	Metallic
Fused pentagons[41]	5 + 12	hexagonal	Metallic
net-W[23]	4 + 6 + 8	orthogonal	Metallic
C_{65}-sheet[26]	5 + 6 + 9	hexagonal	Metallic
C_{41}-sheet[26]	4 + 7	tetragonal	Metallic
Dimerite[25]	5 + 6 + 7	hexagonal	Metallic
Spirographite[42]	6	orthogonal	Metallic

3.3. Electronic properties

The chemical bonding and electronic distribution of porous carbonous C_{18} and $C_{36}H_8$ sheets can be well-understand through the electron localization function (ELF). We first calculate the ELF of porous structures in the numerical range of 0.0 to 1.0 which shows the corresponding low-energy state and electron localization respectively, while 0.5 exhibits the electron gas state. The ELF slices of the plane parallel to *ab* for C_{18} and $C_{36}H_8$ sheets are shown in Fig. 2(a, b), illustrate the strong covalent bonding nature between all carbon atoms. Next, the electronic band structure of porous carbonous allotropes is calculated

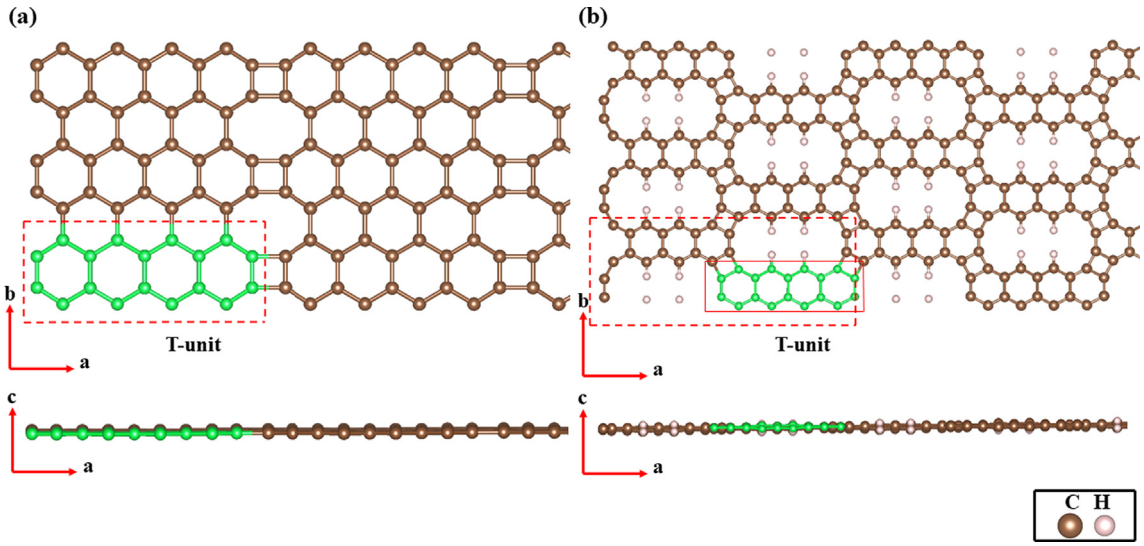

Fig. 1. Atomic configurations of top and side views of (a) C_{18}-sheet and (b) $C_{36}H_8$-sheet. The unit cell is represented by red dashed rectangle and the atoms highlighted with green colors represent the experimentally synthesized tetracene unit (T-unit).

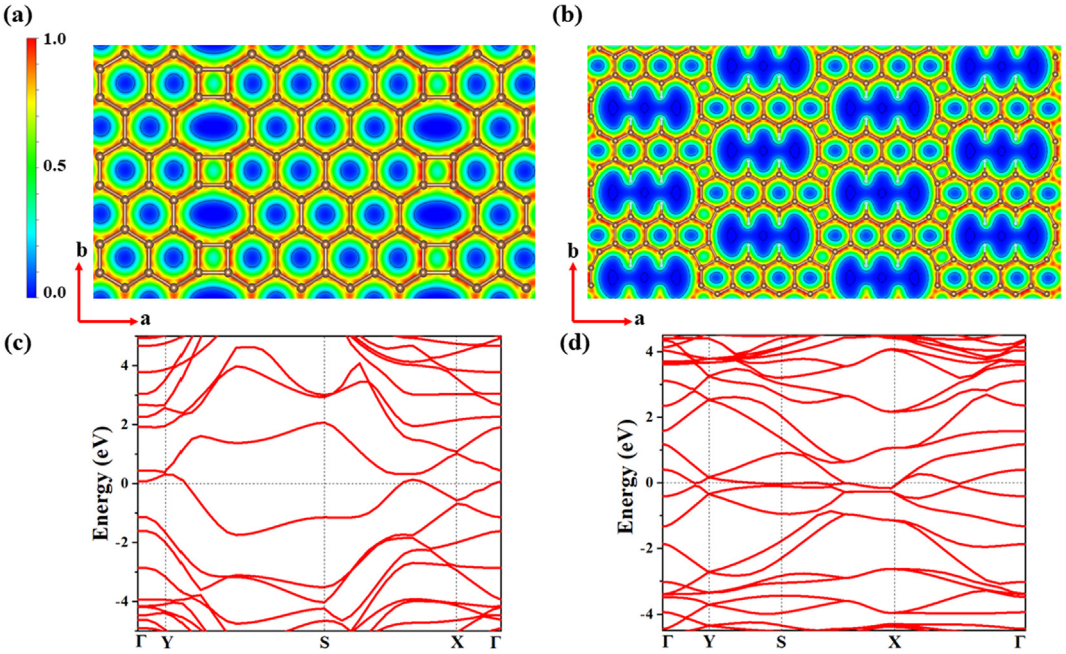

Fig. 2. ELF slices of the plane parallel to *ab* for (a) C_{18}-sheet and (b) $C_{36}H_8$-sheet. The electronic band structure of (c) C_{18}-sheet and (d) $C_{36}H_8$-sheet calculated using HSE06.

using HSE06 functional. The band structures of C_{18} and $C_{36}H_8$ sheets are displayed in Fig. 2(c, d), represents their metallic character with zero band gap. To get more about the electronic conductivity of the under discussion materials, we calculate the total density of states (TDOS). The results are presented in Fig. S3(a, b), demonstrating the participation of atomic orbitals in valence and conduction band from all carbon atoms at the Fermi level, which ensures the excellent conductivity of C_{18} and $C_{36}H_8$ sheets. The metallic character with the intrinsic conductivity of these 2D carbon allotropes enables them as a promising candidate for anode materials of metal-ion batteries (MIBs).

3.4. Application of C_{18} and $C_{36}H_8$ as an anode for Na and K ion batteries

To explore the application of porous carbonous allotropes C_{18} and $C_{36}H_8$ as a promising anode for sodium-ion batteries (SIBs) and potassium-ion batteries (PIBs), the binding strength, theoretical capacity, and mobility of Na and K ions are taken into account. The binding strength of Na and K ions on C_{18} and $C_{36}H_8$ substrates is the basic condition for considering them as anode materials for SIBs and PIBs, so we first investigate the binding energy of single Na/K ions on C_{18}/$C_{36}H_8$ sheets by using the following relation:

$$E_b = (E_{Na/K+(C18/C36H8)} - E_{(C18/C36H8)} - nE_{Na/K})/n \quad (1)$$

where $E_{Na/K+(C18/C36H8)}$ and $E_{(C18/C36H8)}$ are the total energies of Na/K-intercalated and pristine C_{18}/$C_{36}H_8$ structures respectively, and $E_{Na/K}$ is energy per Na/K atoms in the bulk metal and n represents the number of adsorbed atoms. According to the geometrical symmetry of porous C_{18}-sheets as shown in Fig. 3(a) all possible adsorption positions (S_1: the top center of octagonal ring, S_2: the top center of hexagonal ring on the left side of carbon dimer, S_3: the top center of hexagonal ring on the left side of octagonal ring, S_4: on the top center of carbon dimer, S_5: the top center of general hexagonal ring) are taken into account and their corresponding binding energies are (−1.30, −1.20, −1.15, −1.13, and −1.11 eV) respectively. Similarly, for the $C_{36}H_8$-sheet as shown in Fig. 3(b) the adsorption sites (S_1: on the top of right side of big pore, S_2: the top center of hexagonal ring neighbors to carbon dimer, S_3: on the top center of carbon dimer, S_4: on the top of left side of big pore, S_5: on the top of center of big pore) are considered and their corresponding binding energies are (-1.20, −1.18, −1.16, −1.13, and −1.10 eV) respectively. We also calculate the adsorption distance of Na/K ions from the C_{18}/$C_{36}H_8$ substrates corresponding to these sites for analyzing the strength of ions at different positions that can be seen in Table. 2. In order to calculate the charge transfer by Na/K ions adsorbed at the above-discussed sites, we use Bader charge analysis, and their results show that the Na and K ions almost transfer all valence electrons to the C_{18} and $C_{36}H_8$ sheets which indicate the cationic state of Na/K ions. Next, we calculate the charge density difference ($\Delta\rho = \rho_{Na/K+(C18/C36H8)} - \rho_{(C18/C36H8)} - \rho_{Na/K}$) for better illustration of charge transfer from Na/K ions at the first two most stable sites, which verify the results of Bader charge analysis. The results are displayed in Fig. S4(a, b) and S5 (a, b), in which green and blue colors represent the charge gain and charge loss respectively. The net-charge terminology for this case may define as the difference between Bader and nuclear charge of the referent atom.

The rate performance of SIBs and PIBs are mainly determined by the mobility of Na/K ions. We investigate the kinetics of Na and K ions on porous carbonous sheets C_{18} and $C_{36}H_8$ respectively. By following the geometry of the C_{18}-sheet, three representative path-ways are taken for Na-ion diffusion, which can be seen in Fig. 4(a): path-I starts from the top-left of octagonal ring and ends at the top-right of octagonal ring in the same row, path-II: starts from top-left of octagonal ring to the top-left of carbon dimer then moves towards the top-right side of the dimer and further moves from here towards the top-right side of the octagonal ring, path-III: start from the top-left of carbon dimer and ends at top-right of the dimer after passing over the octagonal ring. The diffusion barriers for Na ions corresponding to these pathways are 0.47, 0.46 and 0.49 eV, respectively. In the same way, we take three representative path-ways for K-ion diffusion on $C_{36}H_8$ sheet as shown in Fig. 4(b) path-I starts from the top-center of upper big pore and ends at the top-center of lower big pore, path-II: starts from the top-center of hexagonal ring neighboring to the carbon dimer and ends at the same position in the unit cell repetition, path-III: starts from the top-center of the carbon dimer and ends at the next top-center of carbon dimer which is the same place in the repetition of the unit cell. The diffusion barrier potential corresponding to these path-ways for K-ion is 0.14, 0.12, and 0.029 eV, respectively. The diffusion barrier profiles corresponding to the above-discussed path-ways for C_{18} and $C_{36}H_8$ sheets can be seen in Fig. 5(a, b).

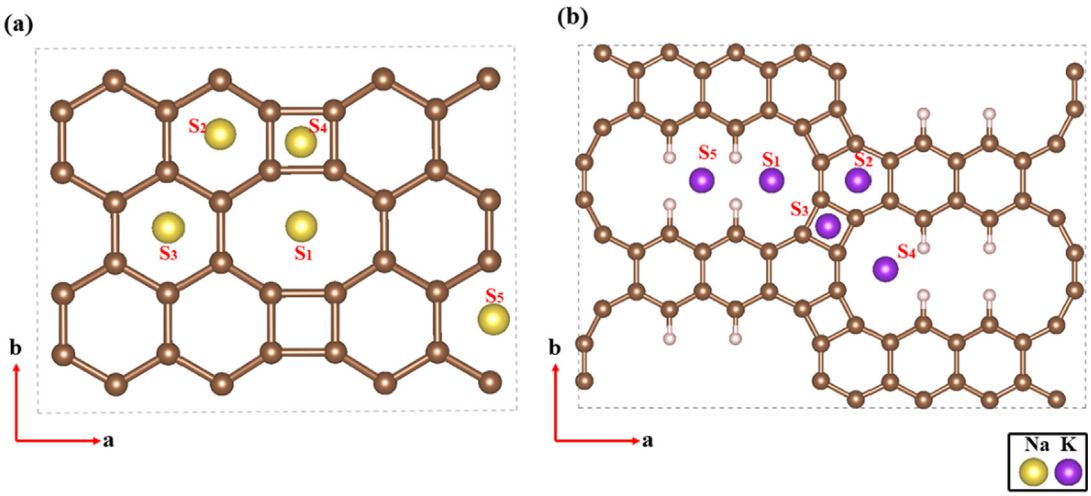

Fig. 3. Top view of (a) Na-ions adsorption on C_{18}-sheet and (b) K-ions adsorption on $C_{36}H_8$-sheet, at five different sites (S_1-S_5).

Table 2
Binding sites (B.S), binding energy (B.E), average adsorption distance (A.D) and charge transfer (Q) of Na/K ions on C_{18} and $C_{36}H_8$-sheets.

C_{18}				$C_{36}H_8$			
B.S	B.E (eV)	A.D (Å)	Q (*e*)	B.S	B.E (eV)	A.D (Å)	Q (*e*)
S_1	−1.30	1.96	0.88	**S_1**	−1.20	2.08	0.91
S_2	−1.20	2.15	0.89	**S_2**	−1.18	2.61	0.90
S_3	−1.15	2.14	0.89	**S_3**	−1.16	2.63	0.91
S_4	−1.13	2.28	0.90	**S_4**	−1.13	2.31	0.91
S_5	−1.11	2.19	0.89	**S_5**	−1.10	2.05	0.90

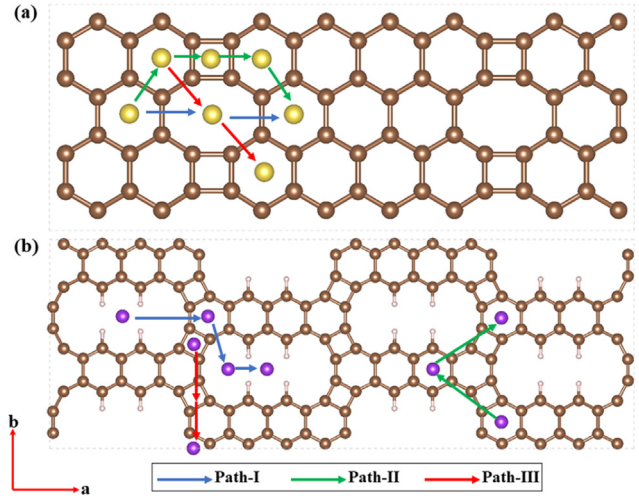

Fig. 4. Three possible migration path-ways for (a) Na-ions diffusion on the C_{18}-sheet and (b) K-ions diffusion on the $C_{36}H_8$ sheet.

The average voltage is essential for having greater energy density and specific capacity which are key parameters to analyze the efficiency of high-performance MIBs. Generally, the average voltage provides an estimation of the net voltage of the system over the range of metal-ion concentrations. We calculate the average voltage for porous C_{18} and $C_{36}H_8$ sheets by using the following relation:

$$V = -[E_{Mn(3D-Si2BN)} - E_{3D-Si2BN} - nE_{M(bulk)}]/Zne \quad (2)$$

where $E_{Mn(C18/C36H8)}$, $E_{C18/C36H8}$, is the energy of the system with and without metal ions, while E_{Mbulk} is the energy of metal ions in the bulk structure and n represent the number of adsorbed metal ions. The average voltage for $C_{18}/C_{36}H_8$ sheets as a function of increasing Na/K ions concentration can be seen in Fig. 6(a, b) which demonstrate that by increasing the metal ions concentration the average voltage gradually decreases because of enhanced repulsive interaction between metal ions and reduced repulsive interaction between substrates and metal ions. The average open-circuit voltage at the full concentration of Na/K ions on $C_{18}/C_{36}H_8$ sheets is 0.12/0.46 V respectively which is comparable to graphene layers (~0.3 V)[44–46], for Na-ions and within the desired range of voltage [0.1,1]V.

Besides, the above-mentioned parameters, the storage capacity is another factor of central importance to analyze high-performance anode materials for battery applications and is the current focus for improvement. The maximum storage capacity of porous carbon C_{18} and $C_{36}H_8$ sheet is calculated by gradually increasing the concentration of Na/K ions on double sides of the sheets. In this regard, six different concentrations of Na/K ions are taken into account. For better understanding, we show the configurations with full capacity of Na and K ions on C_{18} and $C_{36}H_8$ sheets in Fig. S6 and Fig. S7, and their corresponding AIMD results are plotted in Fig. S8 which confirms the thermal stability. Furthermore, by increasing the concentration of metal ions on their corresponding substrates the binding energy gradually decrease which can be seen in Fig. 6(c, d) The estimation of the maximum storage capacity of the studied materials is performed by using the following relation:

$$C = nF/3.6M_{C18/C36H8} \quad (3)$$

where n represents the number of absorbed Na/K ions, F is Faraday constant (96,485.3329 sA mol-1), and M is the mass of unit cell of C_{18} and $C_{36}H_8$. The calculated storage capacities of C_{18} and $C_{36}H_8$sheets for Na and K ions are 991.82 mAh/g and 1277.93 mAh/g respectively, which are significantly greater than commercially available graphite (284 mAh/g) [44], Mo_2C (526 mAh/g) [47], and Ti_3C_2 (351.8) [49] for Na ions as inferred from Table. 3. In short, the intrinsic conductivity, excellent storage capacity and faster kinetics of ions diffusion suggest that porous carbon C_{18} and $C_{36}H_8$ sheets could be high-performance anode materials for Na and K ion batteries.

4. Summary

Based on the first-principle calculation, for the first time, we construct metallic 2D carbon allotropes C_{18} and $C_{36}H_8$ by using tetracene (T) as a repeating building block that has been synthesized recently. The porous 2D C_{18} and $C_{36}H_8$ are composed of 4-6-8 and 4-6-18 carbon rings respectively and show intrinsic conductivity. Most importantly, the monolayers of metallic C_{18} and $C_{36}H_8$ are promising candidates for

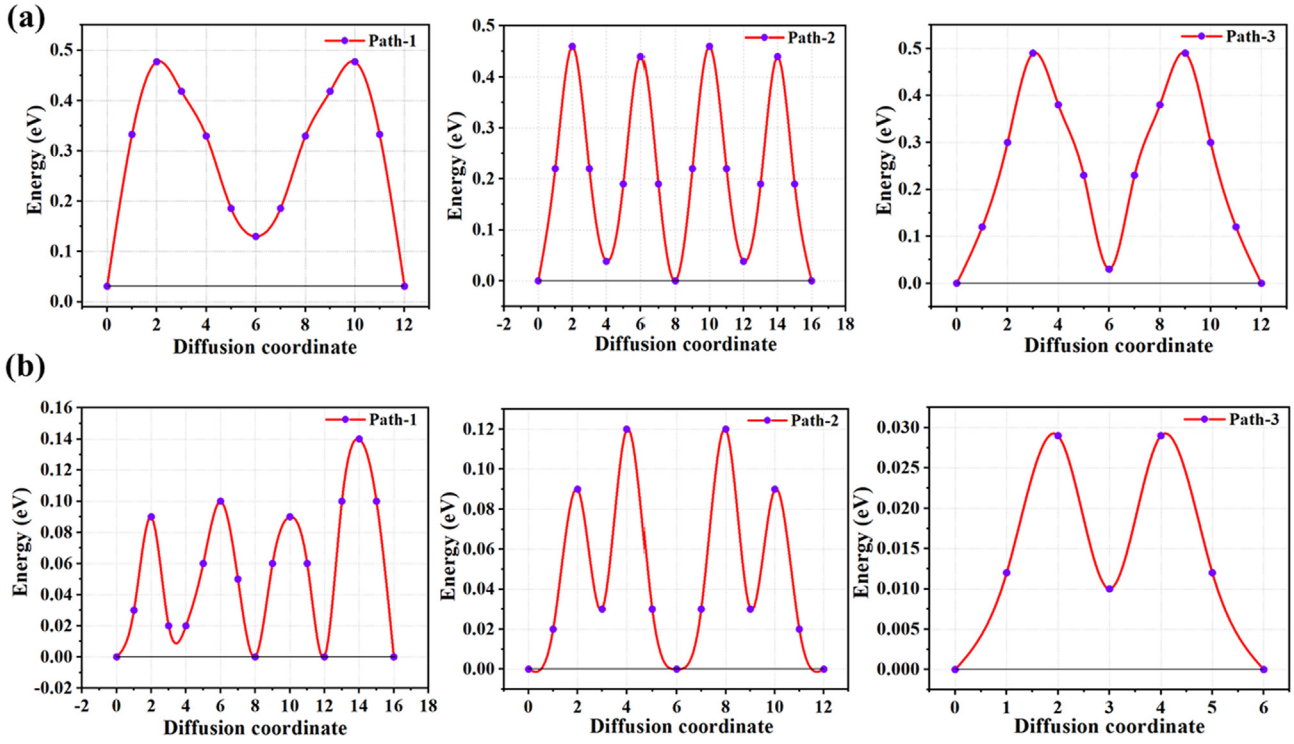

Fig. 5. Diffusion barrier profile of Na-ions on (a) C_{18}-sheet and (b) $C_{36}H_8$-sheet at three different pathways.

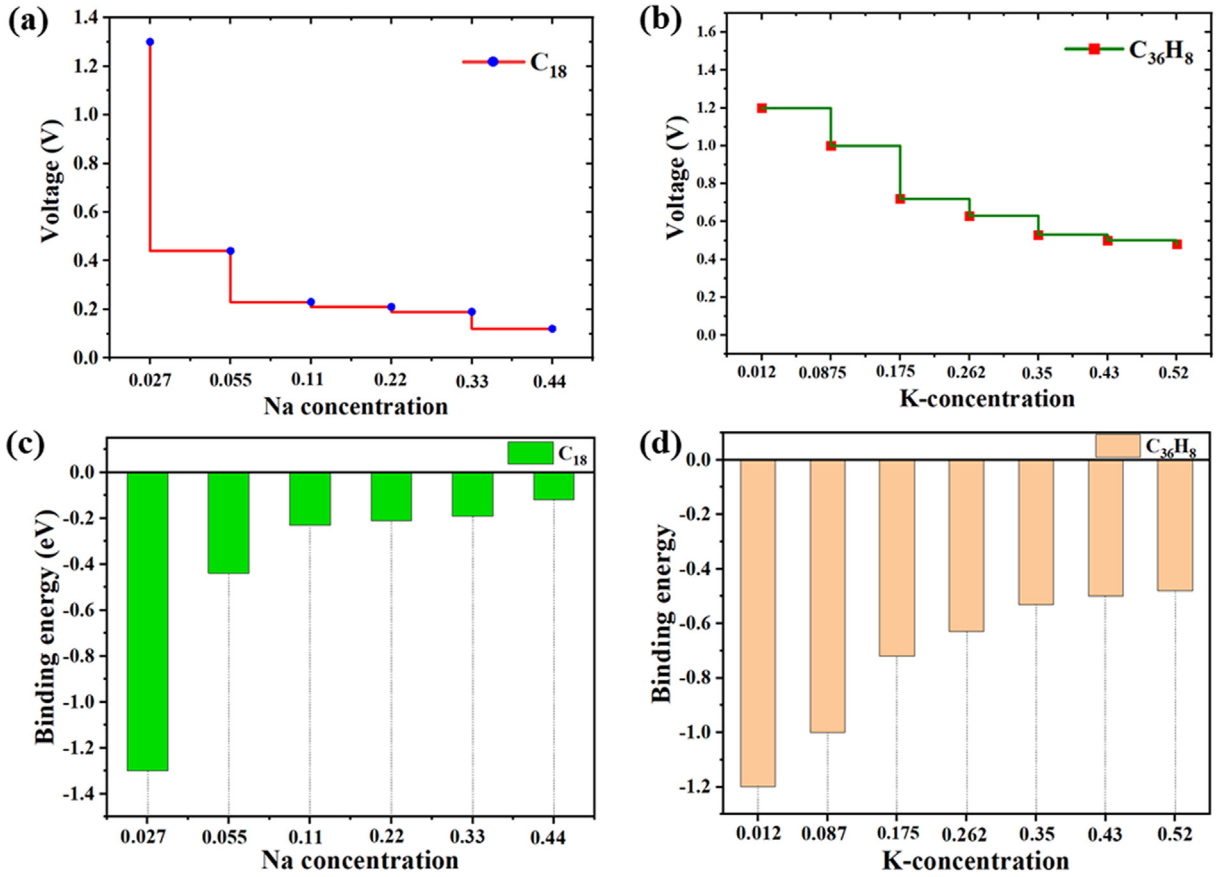

Fig. 6. Average voltage profile of (a) C_{18} sheet and (b) $C_{36}H_8$ sheet. (c) sodium-storage performance at various concentrations on C_{18} sheet. (d) potassium-storage performance at various concentrations on $C_{36}H_8$ sheet.

Table 3
Comparison of specific capacity, migration barrier, average voltage, and the electronic band of C_{18}/$C_{36}H_8$ with other previously reported anode materials for SIBs and PIBs. ('–' means data unavailable).

Materials	Capacity(mAh/g)		Migration barrier(eV)		Voltage(V)		Electronic Band
	(Na)	(K)	(Na)	(K)	(Na)	(K)	
C_{18}	991.82	_	0.46–0.49	_	0.12	_	Metallic
$C_{36}H_8$	_	1277.93	_	0.029–01.4	_	0.46	Metallic
Mo_2C[47]	526	_	0.049	_	0.30	_	Metallic
Boron-graphdiyne[48]	1617	1617	0.28–0.39	0.12–0.32	0.14	0.34	Semiconducting
Ti_3C_2 MXene[49]	351.8	191.8	0.096	0.13	0.13	0.12	Metallic
2D-BC_3[50]	762		0.28		0.44		Semiconducting
GSNS[51]	512	256	0.090	0.050	0.36	0.44	Semiconducting
2D-Electride[52]	1138	_	0.084	_	0.18	_	Metallic

high-performance SIB and PIB, which display the following features: (1) high storage capacity of 991.82 and, 1277.93 mAh/g; (2) low barrier potential 0.46, and 0.029 eV; (3) low average voltage of 0.12 and 0.46 V, respectively. This work not only expands the tetracene-based 2D materials from semiconducting to metallic but also opens a way to design novel carbon materials for high-performance battery applications.

CRediT authorstship contribution statement

Umer Younis: Writing - original draft, Writing - review & editing, Conceptualization, Data curation, Funding acquisition, Formal analysis, Investigation, Methodology, Resources, Project administration, Visualization, and Validation. **Imran Muhammad:** Data curation, Conceptualization, Formal analysis, Resources, Software, Investigation, Methodology, Writing - review and editing. **Y. Kawazoe:** Formal analysis, Conceptualization, Investigation, Data curation, Methodology, Resources, Software, Visualization, and Validation. **Qiang Sun:** Writing - original draft, Writing - review and editing, Investigation, Conceptualization, Methodology, Funding acquisition, Project administration, and Supervision.

Declaration of Competing Interest

The authors declare that they have no known competing financial interests or personal relationships that could have appeared to influence the work reported in this paper.

Acknowledgments

This work is partially supported by grant from the National Natural Science Foundation of China, China. (NSFC-21573008, -21773003), and from the Ministry of Science and Technology of China, China. (2017YFA0204902). Y. K. is thankful to the support by AOARD for the grant of FA2386-18-1-4050. The calculations are supported by the High-performance Computing Platform of Peking University.

Appendix A. Supplementary material

Supplementary data to this article can be found online at https://doi.org/10.1016/j.apsusc.2020.146456.

References

[1] J.Y. Chane-Ching, F. Cobo, D. Aubert, H.G. Harvey, M. Airiau, A. Corma, Chem. - A Eur. J. 11 (2005) 979.
[2] H. Shen, H. Li, L.C. Brinson, Mech. Mater. 40 (2008) 708.
[3] P.M. Tessier, O.D. Velev, A.T. Kalambur, A.M. Lenhoff, J.F. Rabolt, E.W. Kaler, Adv. Mater. 13 (2001) 396.
[4] J. Klett, R. Hardy, E. Romine, C. Walls, T. Burchell, Carbon N. Y. 38 (2000) 953.
[5] Q. Tang, Z. Zhou, Z. Chen, Wiley Interdiscip. Rev. Comput. Mol. Sci. 5 (2015) 360.
[6] J. Gómez-Herrero, F. Zamora, Adv. Mater. 23 (2011) 5311.
[7] I. Tiginyanu, E. Monaico, V. Sergentu, A. Tiron, V. Ursaki, ECS J. Solid State Sci. Technol. 4 (2015) P57.
[8] A. S, MOJ Polym. Sci. 2017, 1, 1.
[9] B. Dou, Q. Hu, J. Li, S. Qiao, Z. Hao, J. Hazard. Mater. 186 (2011) 1615.
[10] Z. Wang, B. Mi, Environ. Sci. Technol. 51 (2017) 8229.
[11] Y. Hou, Z. Wang, J. Guo, H. Shen, H. Zhang, N. Zhao, Y. Zhao, L. Chen, S. Liang, Y. Jin, J. Xu, J. Mater. Chem.A 3 (2015) 23252.
[12] L. Li, T. Wang, Q. Liu, Y. Cao, J. Qiu, Carbon N. Y. 50 (2012) 5186.
[13] J. Mahmood, S.M. Jung, S.J. Kim, J. Park, J.W. Yoo, J.B. Baek, Chem. Mater. 27 (2015) 4860.
[14] S.L. Huang, A.Q. Jia, G.X. Jin, Chem. Commun. 49 (2013) 2403.
[15] S. Zhang, Q. Wang, X. Chen, P. Jena, Proc. Natl. Acad. Sci. U. S. A. 110 (2013) 18809.
[16] X. Li, Q. Wang, P. Jena, J. Phys. Chem. Lett. 8 (2017) 3234.
[17] S. Wang, B. Yang, H. Chen, E. Ruckenstein, J. Mater. Chem.A 6 (2018) 6815.
[18] S. Yu, Y.C. Rao, S.F. Li, X.M. Duan, Appl. Phys. Lett. (2018) 112.
[19] X. Wang, Z. Feng, J. Rong, Y. Zhang, Y. Zhong, J. Feng, X. Yu, Z. Zhan, Carbon N. Y. 142 (2019) 438.
[20] J. Liu, T. Zhao, S. Zhang, Q. Wang, Nano Energy 38 (2017) 263.
[21] U. Arrieta, N.A. Katcho, O. Arcelus, J. Carrasco, Sci. Rep. 7 (2017) 1.
[22] Z. Wang, X.F. Zhou, X. Zhang, Q. Zhu, H. Dong, M. Zhao, A.R. Oganov, Nano Lett. 15 (2015) 6182.
[23] X.Q. Wang, H.D. Li, J.T. Wang, Phys. Chem. Chem. Phys. 15 (2013) 2024.
[24] B. Mandal, S. Sarkar, A. Pramanik, P. Sarkar, Phys. Chem. Chem. Phys. 15 (2013) 21001.
[25] M.T. Lusk, L.D. Carr, Carbon N. Y. 47 (2009) 2226.
[26] H. Lu, S.D. Li, J. Mater. Chem.C 1 (2013) 3677.
[27] C. Su, H. Jiang, J. Feng, Phys. Rev. B - Condens. Matter Mater. Phys. 87 (2013) 2.
[28] Y. Liu, G. Wang, Q. Huang, L. Guo, X. Chen, Phys. Rev. Lett. 108 (2012) 1.
[29] C. Sánchez-Sánchez, C. Sánchez-Sánchez, T. Dienel, A. Nicolaï, N. Kharche, L. Liang, C. Daniels, V. Meunier, J. Liu, X. Feng, K. Müllen, J.R. Sánchez-Valencia, O. Gröning, P. Ruffieux, R. Fasel, Chem. – A Eur. J. 25 (2019) 12074–12082.
[30] U. Younis, I. Muhammad, Y. Kawazoe, Q. Sun, ChemPhysChem 20 (2019) 2799.
[31] I. Muhammad, U. Younis, H. Xie, S. Ahmed, Y. Kawazoe, Q. Sun, Comput. Mater. Sci. 176 (2020) 109529.
[32] F. Wende, M. Marsman, J. Kim, F. Vasilev, Z. Zhao, T. Steinke, Int. J. Quantum Chem. 119 (2019) 1.
[33] V. Shukla, R.B. Araujo, N.K. Jena, R. Ahuja, Nano Energy 41 (2017) 251.
[34] J. Hyed, G.E. Scuseria, M. Ernzzerhof, J. Chem. Phys. 18 (2006) 8207–8215.
[35] H.J.M. James, D. Pack, J. Chem. Inf. Model. 16 (1977) 1748.
[36] A. Allouche, J. Comput. Chem. 32 (2012) 174.
[37] G. Henkelman, B.P. Uberuaga, H. Jónsson, J. Chem. Phys. 113 (2000) 9901.
[38] G. Henkelman, H. Jónsson, J. Chem. Phys. 113 (2000) 9978.
[39] A. Togo, I. Tanaka, Scr. Mater. 108 (2015) 1.
[40] M.A. Blanco, H.W. Hatch, J.E. Cutis, V.K. Shen, J. Chem. Phys. 8 (2018) 084203.
[41] M. Maruyama, S. Okada, Jpn. J. Appl. Phys. 53 (2014) 1.
[42] M.J. Bucknum, R. Hoffmann, J. Am. Chem. Soc. 116 (1994) 11456.
[43] S. Zhang, J. Zhou, Q. Wang, X. Chen, Y. Kawazoe, P. Jena, Proc. Natl. Acad. Sci. U.S.A. 112 (2015) 2372.
[44] Y. Wen, K. He, Y. Zhu, F. Han, Y. Xu, I. Matsuda, Y. Ishii, J. Cumings, C. Wang, Nat. Commun. 5 (2014) 1.
[45] D.A. Stevens, J.R. Dahn, J. Electrochem. Soc. (2001) 148.
[46] K. Gotoh, T. Ishikawa, S. Shimadzu, N. Yabuuchi, S. Komaba, K. Takeda, A. Goto, K. Deguchi, S. Ohki, K. Hashi, T. Shimizu, H. Ishida, J. Power Sources 225 (2013) 137.
[47] D. Çakir, C. Sevik, O. Gülseren, F.M. Peeters, J. Mater. Chem.A 4 (2016) 6029.
[48] I. Muhammad, S. Wang, J. Liu, H. Xie, Q. Sun, J. Renew. Sustain. Energy 11 (2019) 014106.
[49] D. Er, J. Li, M. Naguib, Y. Gogotsi, V.B. Shenoy, A.C.S. Appl, Mater. Interf. 6 (2014) 11173.
[50] C. Ling, F. Mizuno, Phys. Chem. Chem. Phys. 16 (2014) 10419.
[51] F. Li, Y. Qu, M. Zhao, J. Mater. Chem.A 4 (2016) 8905.
[52] J. Hu, B. Xu, S.A. Yang, S. Guan, C. Ouyang, Y. Yao, A.C.S. Appl, Mater. Interf. 7 (2015) 24016.